

Order and dynamics inside H-PDLC nanodroplets: an ESR spin probe study

Corrado Bacchiocchi,[†] Isabella Miglioli,[†] Alberto Arcioni,[†] Ilaria Vecchi,[†] Kashma Rai,[‡]
Adam Fontecchio,[‡] and Claudio Zannoni^{*,†}

*Dipartimento di Chimica Fisica e Inorganica and INSTM, Università, Viale Risorgimento 4, I-40136
Bologna, Italy, and Department of Electrical and Computer Engineering, Drexel University,
Philadelphia PA, 19104, USA*

E-mail: claudio.zannoni@unibo.it

Abstract

We have performed a detailed study of the order and dynamics of the commercially available BL038 liquid crystal (LC) inside nanosized (50–300 nm) droplets of a reflection-mode Holographic Polymer Dispersed Liquid Crystal (H-PDLC) device where LC nanodroplets layers and polymer layers are alternately arranged, forming a diffraction grating. Here, we have determined the macroscopic configuration of the LC local nematic domain director and derived a model of the nanodroplet organization inside the layers. To achieve this, we have taken advantage of the high sensitivity of the electron spin resonance (ESR) spin probe technique, not previously used to study these materials. The spectroscopic analysis was conducted at a series of temperatures ranging from the nematic to the isotropic phase of the LC. In conjunction with SEM images of the H-PDLC cross-section, which provide additional information on the nanodroplet size and shape distribution, the observed director configuration has been modeled as a bidimensional distribution of elongated nanodroplets (prolate ellipsoid) whose long axis is, on the average, parallel to the layers and whose internal director configuration is a quasi-monodomain (“stretched” bipolar) aligned along the nanodroplet long axis. Interestingly, at room temperature the molecules tend to keep an average orientation parallel to the nanodroplet layers even when these are

[†]Università di Bologna

[‡]Drexel University

perpendicular to the magnetic field, suggesting that the molecular organization is dictated mainly by the confinement. This result might explain, at least in part, (i) the need for switching voltages significantly higher and (ii) the observed faster turn-off times in H-PDLCs compared to standard PDLC devices.

Keywords: *surface-induced order; bragg gratings; phase separation, confined liquid crystals*

Introduction

Liquid crystals (LCs) are increasingly used not only in displays but in the preparation of new materials with unconventional properties.^{1,2} Among these LC based materials, polymer dispersed LC (PDLC) composites, where microdroplets of LC are randomly dispersed in a polymer matrix, are of considerable interest, both for technological applications and from a more basic standpoint, because of the possibility of varying their optical properties by applying an external field. In the case of a standard PDLC the size of the LC droplets is larger or comparable to the visible wavelength and the ensuing scattering renders it opaque. A PDLC film placed between two conductive layers can be made to vary from this opaque state to transparent upon application of a field that causes the nematic LC to align and change the observable refractive index so as to match or mismatch that of the polymer matrix. A more recent development is the possibility of using LC dispersions of submicron (100–300 nm) size to prepare rewritable screens for holographic projection. However in Holographically formed PDLCs (H-PDLCs) the LC droplets are arranged in stratified layers alternating with polymer layers.³ Reflection-mode H-PDLCs are reconfigurable Bragg gratings, which reflect a narrow band of incident wavelength and transmit it when the electric field is applied. Index mismatch between the LC and polymer layers results in the reflective property when field is not applied across it. In the field-on state the refractive index becomes uniform, resulting in transmission of the entire incident spectrum. The switchable and reflective properties of H-PDLCs have been studied extensively for applications such as displays,^{4–6} color filters⁷ and optical switches.⁸ To optimize the design of H-PDLCs for diverse applications and improve their switching performance, it is fundamental to characterize the nanodroplet microscopic structure, the LC behavior and the LC–polymer interactions particularly since large changes in physical properties occur due to finite size and confinement effects. To this aim, several microscopic and spectroscopic techniques have been extensively used. SEM and TEM microscopy methods are essential for the nanometer scale structural analysis (see e.g.³ and refs therein) and Nuclear Magnetic Resonance (NMR) has proved to be a suitable technique to study the orientation and

dynamics of the LC inside the polymer matrix.⁹ NMR was used for the first time to study the configuration of directors and dynamics in PDLCs by Golemme et al.^{10,11} Early NMR analysis on PDLC revealed a first order nematic to isotropic (N-I) phase transition for large droplets of LC. For droplets below the critical diameter of ≈ 35 nm, the N-I phase transition showed a continuous variation from an ordered nematic phase to a weakly ordered isotropic phase.¹¹ Iannacchione et al. performed deuteron nuclear magnetic resonance (DNMR) studies on H-PDLCs and surmised that an homeotropic liquid crystal configuration is present at the LC-polymer interface.¹² Their results indicated also a lower orientational order in the nanodroplets compared to the bulk LC. Vilfan et al.¹³ used DNMR and dynamic light scattering (DLS) to study the orientational order and dynamics of a BL038-5CB LC mixture in a H-PDLC. DLS showed that the onset of the nematic phase occurs at a temperature about 40 K lower, compared to the bulk, and takes place gradually. This is possibly due to a polydispersity of nanodroplet sizes having different compositions of non-liquid-crystalline ingredients. DNMR indicated that the structure of the director configuration is macroscopically isotropic and composed by a smaller fraction of a powder-like (low fluidity) nematic polydomain, with high local order, whereas the larger part of the LC is still in the isotropic phase, even at room temperature. However, the bulk BL038 LC, at room temperature, shows a highly ordered nematic phase. The authors suggested that the locally ordered structure is located on the nanodroplet surface, since its contribution to the total DNMR spectrum is small and its translational diffusion is two orders of magnitude slower than that found in the bulk of the droplet cavity.

The lack of NMR results indicating, at least, a small fraction of nematic order along the NMR magnetic field is surprising and appears to be in contrast with the operating principle hypothesized for a H-PDLC device, when a field is applied. To shed further light on the internal nematic director configuration of the nanodroplets, the local molecular order and dynamics, and to compare the observed behavior with that found in the bulk, we propose here the use of the electron spin resonance (ESR) spin probe technique, doping the nematic LC employed with a stable nitroxide radical at a very low ($\approx 10^{-4}$ w/w) concentration and monitoring its spectra in different conditions. This technique, hitherto unused on H-PDLC studies, allows, due to its very high sensitivity, for the direct study of an actual device. Indeed in a preliminar feasibility study we have verified that it is possible to obtain a 100:1 signal-to-noise ratio using a single 20 μm thick H-PDLC cell. Besides, the extremely low concentration of the probe does not introduce a significant perturbation to the system.

The present paper is organized as follows: a brief description of the sample preparation and the exper-

imental methods used is presented in the next section. In the Theory section we summarize the models adopted to simulate the ESR spectra, discussing the typical spectral components included in the analysis. we consider the spectra as a sum of contributions, where each component corresponds to a different “site” (environment) where the spin probe can be located and whose fractional contribution to the ESR spectrum is proportional to its LC molecules population. In the Results section we introduce the model parameters and the schemes employed to recover them from a global analysis. We show that a consistent temperature dependence of the parameters can be achieved only by assuming a multi-site model. In the Discussion section we compare our findings with the results obtained in previous, related studies^{13,14} and we present the combinations of nanodroplet size and shape distribution as well as internal director configuration that are compatible with our results. We conclude trying to draw some technological indications aiming at the improvement of H-PDLC devices.

Experimental Methods

The H-PDLC is prepared by photopolymerization of a prepolymer syrup that consists of tri and hexafunctional oligomers EBECRYL 4866 and EBECRYL 8301 (Cytec, NJ, USA), both at a fraction of 23.85% w/w, 28.4% w/w of LC BL038 (EM Industries, NY, USA) doped with the spin probe, 13.34% w/w photoinitiator (4% w/w Rose Bengal, 10% w/w of coinitiator N-Phenyl Glycine and 86% w/w of N-Vinyl Pyrrolidone) to sensitize the mixture to visible wavelengths and 10.56% w/w surfactant which is used in an actual device to improve the electro optic response. The mixture is placed between two uncoated, alkali free, borosilicate glass slides (display-grade, Corning 1737, Corning, NY, USA), separated by 20 μm spacers forming an approximately 2 mm thick cell. The cell, held by the glass slides at the sides, is then exposed to a 532nm, 5 W, Nd:YAG Verdi laser (Coherent, CA, USA) using a reflection hologram setup to create a reflection grating where the droplet layers are parallel to the glass slides.³ A capillary tube glued to the border of the cell is used to hold it in the chosen position and orientation within the ESR cavity (see experimental scheme in Figure 1). Two types of cells, with same width of 5 mm (the largest dimension fitting inside the dewar tube in the cavity), but different length were manufactured. To maximize the signal, which appeared to be of critical importance in a preliminary series of measurements, the first cell type was 35 mm long to fully span the ESR cavity (25 mm long) with the central, uniformly photo-cured, portion of the cell. Due to its dimensions, this rectangular cell could be rotated around the X axis of the laboratory

frame but not around the Y axis (see scheme in Figure 1). This allowed us to study the anisotropy of the director configuration with respect to a change in the orientation of the nanodroplet layers from parallel (“parallel geometry”, as in the scheme of Figure 1) to perpendicular to the magnetic field (“perpendicular geometry”). To verify our hypothesis that the director configuration is, instead, symmetric with respect to a rotation around an axis perpendicular to the nanodroplet layers (see the Results and the Discussion sections for details), a squared cell, with a length of 5 mm, was prepared. This smaller cell was simply cut out from the rectangular type and could be rotated by 90° around the Y axis by changing the side where the capillary was attached. Due to its smaller dimensions, this cell gave a lower signal that was however still sufficient to clearly show all the features of the spectra.

The BL038 is a commercial LC mixture, with high birefringence, often used in optical devices. In the temperature range 285.2–383.2 K, explored in this study, it exhibits a wide, highly ordered nematic phase ($\langle P_2 \rangle \sim 0.8$ around room temperature) and an isotropic phase. The clearing temperature, T_c , is at 373.2 K, preceded by a N-I coexistence region of about 3 K.

The nitroxide spin probe, used for doping the LC, was the 3β -DOXYL- 5α -cholestane free radical (CSL, Aldrich) which was employed in a number of previous studies^{15–17} where it proved to be a reliable probe of the order and the dynamics of the LC system since it is similar in size, rod-like shape and rigidity to the 5CB LC, which is the main component of the BL038 LC. The CSL structure is shown in Figure 2 together with the chosen ordering (x, y, z , solid line) and magnetic (x', y', z' , dashed line) molecular frames and the indication of its two main reorientational motions, tumbling and spinning, with the corresponding components of the rotational diffusion tensor: D_{\perp} (reorientation of the molecular long axis) and D_{\parallel} (rotation around the long axis), respectively.

The molecular magnetic frame (x', y', z') was chosen according to the standard system of coordinates for the N-O paramagnetic moiety with the x' axis along the N-O bond^{15,18} and the z' axis perpendicular to the five-membered ring, i.e. parallel to the p_z orbital containing the unpaired electron density. According to a standard approach, the z axis of the ordering frame is considered parallel to the principal axis of inertia of the probe (its “long axis”) and, to simplify the rotation which takes the ordering into the magnetic frame,¹⁵ the y axis is considered parallel to the z' axis. To reduce the correlation among variable parameters, the Euler angles, β and γ , between the molecular frames, were fixed in the fits to 15° and 90°, respectively, in agreement with previous results obtained in related systems.^{15–18}

In a preliminary series of measurements and analysis, the signal level was about ten times lower than

the expected one based on the initial amount of CSL added to the H-PDLC syrup, indicating that about 90% of the spin probe free radical was oxidized during the curing process and the subsequent storage of the cell. The signal/noise (S/N) ratio was about 10-15 and was found to be too low to unambiguously assign a given model to each experimental spectrum and determine the corresponding parameters. To allow for a consistent analysis of the spectra, a noise level about five to ten times smaller than the (often relatively small) differences among the calculated lineshapes of competing models was roughly estimated, which corresponded to a required S/N ratio of about 80-100, across the whole temperature range explored.

To compensate for the signal loss, the initial concentration of CSL present in the prepolymer syrup was therefore increased to $6 \times 10^{-3} g_{CSL}/g_{BL038}$ which is six times larger than the limiting concentration typically suggested¹⁹ to avoid Heisenberg spin exchange distortion effects. Typical final spectra had a S/N ratio larger than 100 for the rectangular cells and larger than 40 for the squared cells, with lineshapes essentially identical to the (noisier) spectra obtained in the preliminary set of measurements of H-PDLC cells prepared with $1 \times 10^{-3} g_{CSL}/g_{LC}$, thus indicating the absence of spectral distortions.

We acquired ESR spectra with a Bruker EMX spectrometer equipped with an ER 041XG microwave X-band (9.5 GHz) Gunn Diode bridge and a rectangular ER 4102 cavity. The samples were thermostated with a nitrogen flux through a variable temperature unit Bruker B-VT 2000. The temperature, monitored with a calibrated type T thermocouple (Comark Ltd.) kept in contact with the sample cell, showed a stability better than ± 0.05 K. In a typical acquisition, 100 to 200 scans were averaged to reach the required S/N ratio.

To study the effects due to annealing, spectra recorded from freshly prepared cells were compared with those recorded after either “field cooling” (FC) or “zero field cooling” (ZFC) the sample. This was done by heating it at 353.2 K (above the polymer T_g of 336.0 K, determined by DSC), then slowly cooling it to 323.2 K, approximately 1 K/min, with the magnetic field either set at 6300 G (the highest available on the ESR spectrometer) or turned off, and then equilibrating for 20 min. Finally, the cell was brought to the required temperature for the measurement. The temperature of 323.2 K was a good compromise between having a large fraction of ordered LC molecules (this fraction starts to decrease at higher temperatures) and the highest degree of local order of the LC (which, due to the confinement, decreases at lower temperatures), it was chosen, in a preliminary series of tests, to maximize the effects of annealing. See also the Results and the Discussion sections for further details.

Images of cross-sections of the H-PDLC have been recorded with a Zeiss Supra 50VP SEM, following

the procedure adopted in a previous study¹³ by freeze fracturing the cell and removing the LC with ethanol. Digital image processing was conducted with the Photoshop program to estimate the nanodroplet size and shape distribution.

Theory

The unsaturated, high-field ESR monodomain spectrum $I_m(\omega - \omega_0, \beta_d)$ at frequency ω and at an angle β_d between the director and the spectrometer magnetic field, of the nitroxide spin probe $I_m(\omega - \omega_0, \beta_d)$, is calculated using the classic Stochastic Liouville Equation (SLE) approach of Freed and collaborators^{19–21} which predicts that:

$$I_m(\omega - \omega_0; \beta_d) = \frac{1}{\pi} \langle \langle v | [(\hat{\Gamma} - i\mathcal{L}) + i(\omega - \omega_0)\mathbf{I}]^{-1} | v \rangle \rangle, \quad (1)$$

where the central frequency ω_0 at the spectrometer field $B(0.33T)$ is obtained from the g factor g_0 and the Bohr magneton β_e : $\omega_0 = g_0\beta_e B_0/\hbar$, \mathcal{L} is the Liouville superoperator obtained from the orientation dependent spin Hamiltonian, $\hat{\Gamma}$ is the diffusion superoperator describing the reorientational motion of the probe, $|v\rangle$ is a vector containing spin transition moments averaged over the equilibrium ensemble and \mathbf{I} is the identity. The matrix elements of $\hat{\Gamma}$, assuming the probe reorientation to be diffusional, are^{19–21}

$$\begin{aligned} \langle \langle \sigma_1 | \hat{\Gamma} | \sigma_2 \rangle \rangle &= \delta_{L_1, L_2} \delta_{M_1, M_2} \delta_{K_1, K_2} \delta_{p_1^s, p_2^s} \delta_{q_1^s, q_2^s} \delta_{p_1^I, p_2^I} \delta_{q_1^I, q_2^I} \\ &\times \left\{ D_{\perp} L_1 (L_1 + 1) + (D_{\parallel} - D_{\perp}) K_1^2 \right\}, \end{aligned} \quad (2)$$

where

$$|\sigma_n\rangle \equiv \left(\frac{2L+1}{8\pi^2} \right)^{1/2} D_{M,K}^L(\Omega) |p_n^S, q_n^S; p_n^I, q_n^I\rangle \quad (3)$$

is the spin-orientational space basis set and D_{\parallel} , D_{\perp} are the principal components of the rotational diffusion tensor of the probe for rotations around its long or short axis, respectively. The basis set is obtained from the direct product of the electron spin S with the nuclear spin I eigenfunctions

$$|p^S, q^S; p^I, q^I\rangle \equiv (|S, m_S\rangle \langle S, m'_S|) (|I, m_I\rangle \langle I, m'_I|), \quad (4)$$

while $D_{M,K}^L$ are the orientational Wigner rotation matrices with L, M, K integer; $L \geq 0$; $|M|$ and $|K| \leq L$,

forming the basis set for the orientations. The reorientational motion of the probe is assumed to take place in the local, mean field ordering potential which we assume to be a simple uniaxial $\langle P_2 \rangle$ -type to limit the number of model parameters (see also the Results and the Discussion sections)

$$U(\beta) = -kT \{ \lambda_{20} D_{00}^2(\beta) \}, \quad (5)$$

where λ_{20} is the strength of the potential. The local order is described by the orientational order parameter $\langle P_2 \rangle$ defined as

$$\langle P_2 \rangle \equiv \langle D_{0,0}^2 \rangle = \frac{\int D_{0,0}^2(\beta) \exp[-U(\beta)/kT] \sin \beta \, d\beta}{\int \exp[-U(\beta)/kT] \sin \beta \, d\beta}, \quad (6)$$

where β is the probe orientation with respect to the domain director.

In the complex H-PDLC system we aim to study the orientation of the nematic will hardly be a single monodomain, e.g. due to the surface and local curvature of the nanodroplets and the possibility we have to account for of local domains with different order and fluidity as suggested by the previous DNMR studies [13]. Thus, the experimental ESR spectrum of the H-PDLC samples, $I(\omega - \omega_0)$, was modeled as the weighted sum of several spectral contributions, I_i , corresponding to different “environments” where the CSL spin probe is supposed to be located.

$$I(\omega - \omega_0) = \sum_i f_i I_i(\omega - \omega_0), \quad (7)$$

where f_i is the fractional contribution of the i -th environment.

Besides the monodomain, described above, the environments modeled were: three dimensional, partially ordered polydomain (3DPOP); two dimensional polydomain (2D); isotropic (ISO) and rigid-limit (RL).

In the 3DPOP environment the spin probe is assumed to reorient in a distribution of ordered domains with local director orientation β_d with respect to the magnetic field. The corresponding ESR spectrum, $I_{3DPOP}(\omega - \omega_0)$, is given by the superposition of the monodomain spectra:^{22,23}

$$I_{3DPOP}(\omega - \omega_0) = \int_0^\pi I(\omega - \omega_0; \beta_d) P(\beta_d) \sin \beta_d \, d\beta_d. \quad (8)$$

where, to further limit the number of model parameters, the unknown distribution of the domain directors, $P(\beta_d)$, has been modeled, as it is usually done (e.g. in the EPRL “family” of ESR spectra simulation programs²⁴), by a uniaxial, $\langle P_2 \rangle_d$ -type distribution $P(\beta_d) \propto \exp[\lambda_d P_2(\cos \beta_d)]$ where P_2 is a second rank Legendre polynomial and λ_d is a positive constant. The order of the domain directors is described by the orientational order parameter $\langle P_2 \rangle_d$ defined as

$$\langle P_2 \rangle_d = \frac{\int P_2(\cos \beta_d) \exp[\lambda_d P_2(\cos \beta_d)] \sin \beta_d d\beta_d}{\int \exp[\lambda_d P_2(\cos \beta_d)] \sin \beta_d d\beta_d}. \quad (9)$$

A value of $\langle P_2 \rangle_d = 0$ represents the limiting case of an isotropic distribution of the domain directors, corresponding $P(\beta_d) = 1/\pi$, whereas in the other limit of $\langle P_2 \rangle_d = 1$ the system is a monodomain aligned parallel to the magnetic field with $P(\beta_d) = \delta(\beta_d)$.

The 2D environment is modeled similarly to the 3DPOP one by changing the angular volume element from $\sin \beta_d$ to $d\beta_d$

$$I_{2D}(\omega - \omega_0) = \frac{1}{\pi} \int_0^\pi I(\omega - \omega_0; \beta_d) d\beta_d. \quad (10)$$

The ISO contribution is calculated by setting at zero the strength of the ordering potential, λ_{20} whereas a simpler approach is adopted for the RL component which is modeled as a powder spectrum where reorientational relaxation effects are neglected (see e.g.²² and refs. therein).

Results

Final ESR spectra were recorded across the temperature interval 285.2–383.2 K which was chosen to be wide enough to study all the significant spectral changes exhibited by the system, as determined from a series of preliminary spectra. Due to the unavoidable loss of signal, after about 1-2 weeks of measurements, it was not possible to record all the required spectra from a single H-PDLC cell. In the end, four rectangular and two squared cells (see the Experimental section for details) were used to cover different, partially overlapping portions of the chosen temperature interval. Spectra of different cell replicas (even when prepared from separate batches of the prepolymer syrup) recorded at the same temperature and after the same temperature treatment (i.e. FC or ZFC) were completely reproducible i.e. they were identical or exhibited very small differences.

Figure 3, uppermost plot, shows a typical ESR spectrum of the H-PDLC cell at 285.2 K, recorded in the

parallel geometry (\parallel) after FC also in the parallel geometry (green line), compared to a typical rigid-limit spectrum of the cell recorded at 153.2 K in the parallel geometry (black, solid line). Despite the relatively large difference in temperature, the spectrum at 285.2 K appears to have some key features in common with the rigid-limit one, suggesting that at least a fraction of the CSL spin probe is located in a rigid-limit environment. Spectra at 285.2 K of the freshly prepared cell or after ZFC, also recorded in the parallel geometry (not shown), were only slightly different to the one after FC. The spectrum recorded immediately after a 90° rotation of the FC cell (i.e. in the perpendicular geometry: Figure 3, lowermost plot, green line) was clearly different, revealing the presence of an anisotropic contribution which did not realign along the magnetic field. In a series of preliminary analysis, these FC parallel and perpendicular spectra were globally fitted to a 3-site model (rigid-limit + 3DPOP + isotropic), but the recovered best fit $\langle P_2 \rangle_d$ was inconsistent being essentially zero for the parallel spectrum but very close to unity for the perpendicular, as if a monodomain contribution, perpendicular to the magnetic field, was present. The spectra could be instead consistently modeled (red line) by replacing both the isotropic and 3DPOP components with a bidimensional (2D) distribution of local nematic LC domains, in the assumption that the symmetry axis of the distribution is perpendicular to the nanodroplet layers and that the distribution rotates “as a whole” with the cell in the magnetic field. The best-fit components of this 2-site model are shown in the three central plots of Figure 3. The rigid-limit contribution (RL, black, dashed line), being isotropic, is unaffected by the 90° rotation whereas the bidimensional contribution changes from parallel (2D \parallel , blue line) to perpendicular (2D \perp , cyan line). By adopting this model, a consistent temperature dependence of the best-fit parameters was recovered from the global analysis of the parallel and perpendicular spectra recorded in the temperature range 285.2–308.2 K, after FC in the parallel geometry. Results of the fits are presented in Figure 4 (experimental: dashed lines, fits: solid lines; \parallel , \perp : parallel and perpendicular geometry, respectively) and show excellent agreement with experiment.

The lineshapes of ESR spectra at higher temperatures, recorded in the parallel geometry after FC also in the parallel geometry (see, e.g., spectrum at 353.2 K in Figure 5, experimental: dashed lines, fits: solid lines), appeared to correspond to a nematic monodomain contribution superimposed to the typical three peaks of a relatively fast motional isotropic spectrum. Indeed, in the temperature interval 345.2–373.2 K, a consistent temperature dependence of the best-fit parameters was obtained by adopting a 3-site model composed by a nematic monodomain, an isotropic and a, still present, rigid-limit contribution. In the interval 337.2–343.2 K, a more consistent behavior of the parameters was obtained by replacing the

nematic monodomain contribution with a three dimensional, partially ordered polydomain (3DPOP) and the isotropic contribution with a 2D distribution with low local $\langle P_2 \rangle$ (whose contribution is, in fact, similar to the isotropic one). Results of the fits are presented in Figure 5 (experimental: dashed lines, fits: solid lines). The lineshapes of the nematic monodomain contribution decrease at increasing T becoming barely visible at 373.2 K, where its fraction is estimated to be lower than 10 %. Above 373.2 K the sample is fully isotropic.

The analysis of the FC spectra recorded in the temperature region 313.2–335.2 K proved to be the more difficult one, since all the spectral components described so far are present. In a preliminary series of fits, a 4-site model, composed by a rigid-limit, 2D, 3DPOP and isotropic contributions was tested. The isotropic component was poorly determined and it showed large correlations with the 2D component. A 3-site model composed by a rigid-limit, 2D and 3DPOP component was then adopted. This simpler model provided more stable best-fit parameters with a consistent temperature dependence.

In the temperature range 285.2–353.2 K, the spectra recorded in the parallel and perpendicular geometry could be globally fitted to the same values of the fractions of the components, local $\langle P_2 \rangle$ and dynamics, in the assumption that the ordered fraction did not realign along the magnetic field after the 90° rotation. Individual (not global) analysis of the spectra in the perpendicular geometry indeed indicated that the ordered fraction rotated as a whole with the sample, remaining essentially unaffected by the magnetic field up to 353.2 K. At 357.2 K, the best-fit local $\langle P_2 \rangle$ decreased from 0.60, before the rotation, to 0.31 after it and at higher temperatures the order of the nematic fraction was completely disrupted, becoming isotropic. At all the temperatures studied, spectra recorded immediately after the rotation and two hours later were identical.

Figure 6 shows the spectral changes observed at 353.2 K upon the 90° rotation from the parallel (uppermost plot) to the perpendicular (lowermost plot) geometry (green line: experimental, red line: fit to the 3-site model described above, RL + ISO + N || or N ⊥). The best-fit components of the model are shown in the three central plots of Figure 6: nematic contribution to the parallel or perpendicular spectrum (N ||, blue line and N ⊥, cyan line) and isotropic contribution (ISO, black, dashed line) assumed identical in the two fits. For clarity, the smaller fraction of the rigid-limit contribution is not shown.

The fractional contribution of the ordered component was always larger after FC the sample compared to ZFC. In particular, the effects of annealing the cell in the magnetic field were more evident in an intermediate temperature region (\approx 310–350 K) and decreased at the lowest and highest temperatures.

Figure 7, upper plot, shows a comparison between the spectra recorded after ZFC or FC the same replica at 323.2 K (black and green lines, respectively). The spectrum of the FC sample exhibits a clear increase of the peaks closer to the central one, in keeping with the increase of the ordered component. Both spectra could be globally fitted to the same local $\langle P_2 \rangle$ and dynamics but with different fractional contribution of the 3DPOP component. The experimental spectrum after FC (green line) and the fit to a 3-site model (red line) are shown in the lower plot, together with the three components: rigid-limit (RL, black, dashed line), bidimensional (2D, blue line) and 3DPOP (cyan line).

The temperature dependence of the fractions, f_i , of the various spectral contributions is shown in Figure 8 (lines are a guide for the eye). As the temperature increases, the rigid-limit fraction decreases and its distinctive peak around 3363–3364 G, where no other signal is present, is clearly visible up to 365.2 K in the spectra with the best S/N ratio (see Figure 5). Above this temperature and up to 373.2 K, the peak becomes comparable to the noise and even if it seems to be still present, its contribution of about 5–10 %, recovered from the analysis, bears relatively large uncertainty. The fractional contribution of the 2D component is approximately constant up to 308.2 K, then it begins to decrease when a more ordered 3DPOP component appears. At 345.2 K this component becomes a nematic monodomain (N) and decreases approximately linearly with the temperature. The local order of the 2D component (see Figure 9) oscillates around very small values between 328.2 and 343.2 K, thus becoming similar to an ISO component. Only above 343.2 K the best-fit, local $\langle P_2 \rangle$ of the 2D component becomes constantly very close to zero. Starting at 345.2 K the 2D contribution is therefore replaced with an ISO component which increases and becomes the only contribution present above the bulk T_c .

In Figure 9 the local $\langle P_2 \rangle$ of the ordered components (thinner, dashed lines are a guide for the eye) is compared to that observed in the bulk BL038 LC. Figure 10 shows the temperature dependence of the rotational diffusion tensor, D_{\perp} , of the various components (thinner, dashed lines are a guide for the eye) together with a comparison to the bulk BL038 LC (values close to the T_c , in the bulk BL038 N-I coexistence region, have been removed).

The effect of a 90° rotation of the squared H-PDLC cells around the Y axis was studied at 323.2 K, after FC. At this temperature the 3DPOP contribution is approximately at its maximum and the dynamics is still relatively slow. These conditions would therefore tend to maximize possible differences due to an anisotropy of the director configuration with respect to this rotation. Spectra recorded before and after the rotation (not shown) were, instead, identical and very similar, albeit relatively noisier, to those taken at the

same temperature, after FC, from the rectangular cells (see, e.g., Figure 7, FC plot).

Figure 1 shows a SEM image of the sample cross-section. The nanodroplet layers are clearly visible as parallel arrangements of darker areas separated by brighter, pure polymer layers. A digital analysis of the image reveals that the nanodroplet size and shape is quite variable. The size range is estimated to be about 50–300 nm. The general shape is irregular rather than uniformly spherical and appears to be, on the average, stretched along the layers. In particular, the direction of the elongation seems to be parallel rather than perpendicular to the layers.

We would like to point out that even if the modeling is apparently complicated, all the parameters can be unambiguously recovered from the global fits since the experimental data and their temperature dependence are sensitive to this level of detail.

Discussion

The consistency of the ESR spectra of different replicas of the H-PDLC sample cells, even when comparing replicas prepared from separate batches, indicated the high reproducibility of the process involving their manufacturing and photocuring. When differences were present, they were always very small, tended to decrease at increasing temperature and could be consistently interpreted, in the analysis, in terms of the same local order and dynamics but a slightly different temperature treatment of the sample (FC or ZFC), resulting, e.g., in a slightly different $\langle P_2 \rangle_d$ of the local nematic domain director distribution or in a different (< 5%) fractional contribution of the spectral components considered in the fitting model.

The spectral analysis indicates that the director configuration inside the H-PDLC nanodroplets is more complex than what has been previously found^{9,10,12,13} and provide new evidence, at the molecular scale, to further narrow the range of possible models describing the anisotropy of the droplet size and shape, their orientational distribution within the layers and their internal director configuration.

At the lowest temperature studied, 285.2 K, our results seemed to be in agreement with those obtained by Vilfan et al.¹³ who reported the presence of a rigid-limit (powder-like) and an isotropic contribution, but the clear difference observed between spectra recorded in the parallel and the perpendicular geometry (rotation of the sample cell around the laboratory X axis, see Figure 1, upper part), in the temperature range 285.2–373.2 K, clearly indicated the presence of a macroscopically anisotropic contribution, not observed before. At 285.2 K the FC, parallel spectrum was only slightly different from that recorded

after ZFC or that of a freshly prepared cell. In an intermediate temperature range ($\approx 310\text{--}350\text{ K}$), the differences between FC and ZFC or the fresh cell were the largest and tended to decrease again at higher temperatures. This behavior suggests a model where, at the lowest temperatures, the director configuration is governed mainly by the confinement and is, therefore, less sensitive to the annealing, whereas at higher temperatures, due to increased mobility, the molecules (or, at least, a certain fraction of them) will align along the magnetic field, without the need of the annealing, to form a 3DPOP or a nematic monodomain. In the intermediate temperature region, between the confinement-induced and the field-induced director configuration, FC the sample produces the largest effects.

The nature of the suggested confinement-induced director configuration, which appears to be present up to a certain temperature, can be further understood by considering that the ordered fraction, observed in the parallel spectra, did not realign along the magnetic field in the perpendicular ones, but instead either rotated “as a whole” with the sample (up to 353.2 K) remaining essentially unaffected by the field, or was disrupted by the field, becoming isotropic (above 357.2 K). Spectra recorded two hours after the rotation or after a sequence of up to four FC in the perpendicular geometry did not show any significant change, suggesting that the field is not able to induce an alignment perpendicular to the layers.

Spectra recorded before and after a 90° rotation of the cell around an axis perpendicular to the layers (Y axis, Figure 1, lower part) were, instead, identical, in agreement with an axial symmetry of the local nematic domain directors around the Y axis.

Model for the director configuration inside the droplets

Our models do not make assumptions about the preferred orientation of the LC at the droplet surface. Several authors have suggested that the addition of a surfactant, present also in our case, should favor an homeotropic orientation.³ Our only assumption, in this respect, is that the rigid-limit contribution is due to CSL located in the fraction of the LC molecules close to the droplet inner surface whereas the interior of the nanodroplets shows a larger mobility. It is also important to recognize that the ESR data do not reveal whether the different environments, where the CSL can be located, coexist within each droplet. From this point of view, there might be nanodroplets entirely rigid-limit, even if this seems rather unlikely, and other nanodroplets fully isotropic or 3DPOP. We can instead examine the various arrangements of the different domains inside the same droplet. First we notice that the assumption of an equilibrium, within the same droplet, between the isotropic fraction and the 3DPOP–N contribution does not seem to be compatible

with our results. In such a model, in fact, the ordered fraction should conceivably occupy the “core” of the droplet to minimize the energy that would be otherwise much larger if this ordered fraction were in direct contact with the surface layer. Such an ordered core surrounded by an isotropic region, with a mobility of the same order of magnitude of that observed in the bulk (see Figure 10), should be reoriented by the magnetic field, at least partially. Our rotation tests (see also next section) clearly indicated, instead, that the sample did not reorient along the field.

In our model, we thus postulate an equilibrium between LC molecules forming a layer on the droplet surface, with a very limited mobility, and molecules in the remaining volume, the droplet cavity, with a faster dynamics. At each T , the local $\langle P_2 \rangle$, the $\langle P_2 \rangle_d$ of the director distribution and the T_c depend on the size and shape of the cavity, which, in turn, depends on the size and shape of the droplet and on the thickness of the interfacial layer. As the T increases, less and less molecules remain “frozen” on the surface layer, thus increasing the size of the cavity. At the same time, an increasing fraction of nanodroplets reaches the T_c thus becoming isotropic.

The director configuration at each temperature can be viewed as the result of a different equilibrium between two limiting situations. Above a certain dimension of the cavity, the surface-induced distortions to the LC structure in the cavity are negligible, the director configuration is bipolar, oriented along the axis of the elongated droplet, with a bulk like local $\langle P_2 \rangle$. Upon FC, a monodomain, oriented along the magnetic field, can be formed. Below a certain dimension of the cavity, the bipolar director configuration is distorted by surface effects and the local $\langle P_2 \rangle$ is lower compared to the bulk. Upon FC, the bipolar configuration can be annealed, thus improving the alignment along the axis of the droplet.

Model for the nanodroplet distribution

In the assumption of a bipolar LC director configuration inside the nanodroplets, the observed 2D distribution of local nematic domains would be compatible with an H-PDLC structure where the layers are formed by elongated nanodroplets whose main axis is parallel to the layers and is randomly oriented in a bidimensional distribution (see Figure 11).

On the other hand, by assuming a bidimensional director configuration inside each nanodroplet, the resulting macroscopic director distribution would be compatible with that observed experimentally only if all the nanodroplets were elongated perpendicularly to the layers, but clearly this would not be compatible with what can be observed from the SEM images (see Figure 1).

At higher temperature, the bipolar director configuration, present inside a fraction of the nanodroplets, can be more easily aligned along the magnetic field when this is parallel to the layers.

Conclusions

The molecular organization and the local fluidity of the BL038 liquid crystal (LC) inside the nanosized droplets of an actual reflection-mode Holographic-PDLC (H-PDLC) cell have been analyzed in detail. Using the ESR spin probe technique, we found for the first time evidence of the presence of a fraction of LC molecules with a macroscopically anisotropic LC director configuration. The main experimental support to this was the consistent difference between ESR spectra of field cooled samples recorded in the parallel and perpendicular geometry which could be observed in the temperature range 285.2–373.2 K (the BL038 LC bulk T_c). This result extends previous NMR studies^{12,13} which found an immobilized LC fraction, close to the polymer surface, and an isotropic fraction. The main findings from the ESR measurements combined with the inspection of the SEM images are compatible with a bipolar LC director configuration inside elongated nanodroplets. These findings are:

(i) a global analysis of spectra recorded in the parallel and perpendicular geometry between 285.2 and 308.2 K clearly indicates that the macroscopic LC director configuration is unaffected by the magnetic field and has an axial symmetry with the local nematic domain director uniformly distributed along the nanodroplet layers.

(ii) between 313.2 and 373.2 K, only in the parallel geometry, a fraction of the LC molecules forms a partially ordered polydomain aligned along the magnetic field, and hence along the layers, which at 345.2 K becomes a nematic monodomain. When the sample is oriented in the perpendicular geometry, this aligned contribution either maintains the orientation along the layers, retaining almost the same local order (up to about 353.2 K), or it becomes isotropic (above 357.2 K);

(iii) SEM images indicate that the nanodroplet shape is, on the average, elongated (prolate ellipsoid), having the direction of the elongation (nanodroplet axis) preferentially parallel to the layers.

The lack of alignment along a direction perpendicular to the droplet layers (the direction of the so called “grating vector”³) appears to be in contrast with the usual operational geometry of a reflection-mode H-PDLC device, where the electric field-induced alignment should form a monodomain perpendicular to the droplet layers. Moreover, the analysis showed that the local nematic order in the H-PDLC at room

temperature is smaller than that observed in the bulk BL038 LC. We believe that these findings can explain the rather large electric field needed to switch an H-PDLC device, compared to a standard PDLC device.

The reflection-mode H-PDLC technology might be improved by avoiding the LC preferred orientation along the nanodroplet layers, observed at room temperature, which requires a relatively large electric field to be switched to a monodomain perpendicular to the layers. A possible strategy might be that of removing the axial symmetry of the director configuration by favoring, e.g., a three-dimensional polydomain director field. A key element, in such a device, would be the presence of spherical, instead of elongated, nanodroplets.

Acknowledgement

We thank MIUR, INSTM, EU and the University of Bologna for support. We also thank Dr. Gregor Skačej for useful discussions and the Drexel University's Centralised Research Facility (CRF), where the SEM images were obtained.

References

- (1) *Liquid Crystals Applications and Uses*; Bahadur, B., Ed.; World Scientific Publishing Co.: River Edge, NJ, 1995; Vol. 3.
- (2) Woltman, S. J.; Jay, G. D.; Crawford, G. P. *Nature Materials* **2007**, *6*, 929.
- (3) Bunning, T. J.; Natarajan, L. V.; Tondiglia, V. P.; Sutherland, R. L. *Annu. Rev. Mater. Sci.* **2000**, *30*, 83.
- (4) Tanaka, K.; Kato, K.; Tsuru, S.; Sakai, S. *J. Soc. Inf. Disp.* **1994**, *2*, 37.
- (5) Fontecchio, A. K.; Bowley, C. C.; Chmura, S. M.; Li, L.; Faris, S.; Crawford, G. P. *J. Opt. Tech.* **2001**, *68*, 652.
- (6) Qi, J.; Crawford, G. P. *Displays* **2004**, *25*, 177.
- (7) Yeralan, S.; Gunther, J.; Ritums, D.; Cid, R.; Popovich, M. *Opt. Eng.* **2002**, *41*, 1774.
- (8) Domash, L.; Crawford, G. P.; Ashmead, A.; Smith, R.; Popovich, M.; Storey, J. *Society of Photo-Optical Instrumentation Engineers* **2000**, *4107*, 46.

- (9) Vilfan, M.; Vrbancic-Kopac, N. In *Liquid Crystals in Complex Geometries*; Crawford, G. P., Žumer, S., Eds.; Taylor & Francis: London, 1996; Chapter 7, pp 159–186.
- (10) Golemme, A.; Žumer, S.; Doane, J. W.; Neubert, M. E. *Phys. Rev. A* **1988**, *37*, 559.
- (11) Golemme, A.; Žumer, S.; Allender, D. W.; Doane, J. W. *Phys. Rev. Lett.* **1988**, *61*, 2937.
- (12) Iannacchione, G. S.; Finotello, D.; Natarajan, L. V.; Sutherland, R. L.; Tondiglia, V. P.; Bunning, T. J.; Adams, W. W. *Europhys. Lett.* **1996**, *36*, 425.
- (13) Vilfan, M.; Zalar, B.; Fontecchio, A. K.; Vilfan, M.; Escuti, M. J.; Crawford, G. P.; Žumer, S. *Europhys. Lett.* **2002**, *66*, 021710–1.
- (14) Jazbinšek, M.; Drevenšek Olenik, I.; Zgonik, M.; Fontecchio, A. K.; Crawford, G. P. *J. App. Phys.* **2001**, *90*, 3831.
- (15) Meirovitch, E.; Freed, J. H. *J. Phys. Chem.* **1984**, *88*, 4995.
- (16) Arcioni, A.; Bacchiocchi, C.; Vecchi, I.; Venditti, G.; Zannoni, C. *Chem. Phys. Lett.* **2004**, *396*, 433.
- (17) Vecchi, I.; Arcioni, A.; Bacchiocchi, C.; Tiberio, G.; Zanirato, P.; Zannoni, C. *J. Phys. Chem. B* **2007**, *111*, 3355.
- (18) Carr, S. G.; Khoo, S. K.; Luckhurst, G. R.; Zannoni, C. *Molec. Cryst. Liq. Cryst.* **1976**, *35*, 7.
- (19) Freed, J. H. Theory of slow tumbling ESR spectra for nitroxides. In *Spin Labeling. Theory and Applications*; Berliner, L. J., Ed.; Academic Press: New York, 1976; Chapter 3, p 53.
- (20) Freed, J. H. ESR lineshapes and saturation in the slow motional region. The stochastic Liouville approach. In *Electron Spin Relaxation in Liquids*; Muus, L. T., Atkins, P. W., Eds.; Plenum Press: New York, 1972; Chapter 14, p 387.
- (21) Schneider, D. J.; Freed, J. H. Calculating slow motional magnetic resonance spectra: a user's guide. In *Biological Magnetic Resonance. Spin Labeling*; Berliner, L. J., Reuben, J., Eds.; Plenum Press: New York, 1989; Vol. 8, Chapter 1, p 1.
- (22) Zannoni, C.; Pedulli, G. F.; Masotti, L.; Spisni, A. *J. Mag. Res.* **1981**, *43*, 141.
- (23) Meirovitch, E.; Nayeem, A.; Freed, J. H. *J. Phys. Chem.* **1984**, *88*, 3454.

- (24) Budil, D. E.; Lee, S.; Saxena, S.; Freed, J. H. *J. Mag. Res.* **1996**, *120*, 155.

FIGURE CAPTIONS

Figure 1. Scheme and laboratory reference frame of the ESR measurements. (a) placement of the rectangular cell inside the instrument cavity in the parallel (left) or perpendicular (right) geometry. (b): placement of the squared cell. (c) scanning electron micrograph of a cross-section of the H-PDLC used in the ESR measurements. Parallel arrangements of darker areas are the nanodroplet layers clearly separated by brighter, pure polymer layers. The grating spacing is about 300 nm.

Figure 2. Chemical structure of the CSL spin probe together with the chosen ordering (xyz , solid line) and magnetic ($x'y'z'$, dashed line) molecular frames, the tilt angle, β , and the principal components, D_{\perp} (reorientation of the molecular long axis) and D_{\parallel} (rotation around the molecular long axis), of the rotational diffusion tensor.

Figure 3. Uppermost plot: typical ESR spectrum of the H-PDLC cell recorded at 285.2 K, after field cooling (see text for details), in the parallel geometry (green line), compared to a typical rigid-limit spectrum recorded at 153.2 K (black, solid line), and fit (RL + 2D \parallel , red line) to a model formed by two contributions, one is rigid-limit (RL, black, dashed line) the other is a bidimensional director distribution (2D \parallel , blue line). Lowermost plot: spectrum of the H-PDLC cell after a 90° rotation to the perpendicular geometry (green line) and fit (RL + 2D \perp , red line) to the same model, in the assumption that only the bidimensional contribution has changed (2D \perp , cyan line), whereas the rigid-limit contribution, being isotropic, is unaffected by the rotation.

Figure 4. Temperature dependence of typical experimental ESR spectra (dashed line) and fits to a 2-site model (bidimensional + rigid-limit, solid line) recorded, after field cooling (FC), in the parallel geometry (\parallel) and then rotated to the perpendicular geometry (\perp). Spectra did not change after subsequent FC in the perpendicular geometry (see text for details).

Figure 5. Temperature dependence of typical experimental ESR spectra recorded in the parallel geometry, after field cooling (dashed line) and fits (solid line) to a 3-site model (337.2–343.2 K: RL + 3DPOP + 2D, 345.2–373.2 K: RL + N + ISO) or to a single site, isotropic model (383.2 K).

Figure 6. Uppermost plot: typical ESR spectrum of the H-PDLC cell recorded at 353.2 K, after field cooling, in the parallel geometry (green line) and fit to a 3-site model (RL + ISO + N \parallel , red line) formed by a rigid-limit, an isotropic (ISO, black, dashed line) and a nematic monodomain (N \parallel , blue line) contribution. Lowermost plot: spectrum of the H-PDLC cell after a 90° rotation to the perpendicular geometry (green line) and fit to the same model (RL + ISO + N \perp , red line), in the assumption that only the nematic monodomain contribution has changed (N \perp , cyan line). For clarity, the smaller fraction of the rigid-limit contribution is not shown.

Figure 7. Upper plot: typical ESR spectra at 323.2 K of a zero field cooled (ZFC, black line) and a field cooled (FC, green line) H-PDLC cell. Lower plot: FC experimental spectrum (same green line of the upper plot) and fit to a 3-site model (red line) formed by a rigid-limit (RL, black, dashed line), a bidimensional (2D, blue line) and a three dimensional, partially ordered polydomain (3DPOP, cyan line) contribution.

Figure 8. Temperature dependence of the fractional contribution, f_i , to the ESR spectrum of the observed spectral components. Lines are a guide for the eye. The vertical line at 373.2 K indicates the bulk BL038 liquid crystal T_c .

Figure 9. Temperature dependence of the local orientational order parameter, $\langle P_2 \rangle$, of the bidimensional (2D), partially ordered polydomain (3DPOP) and nematic monodomain (N) components (see text for details) compared to the bulk BL038 liquid crystal. Thinner, dashed lines are a guide for the eye. The vertical line at 373.2 K indicates the bulk BL038 T_c .

Figure 10. Temperature dependence of the tumbling diffusion coefficient, D_{\perp} , of the bidimensional (2D), partially ordered polydomain (3DPOP), nematic monodomain (N) and isotropic (ISO) components (see text for details) compared to the bulk BL038 liquid crystal. Thinner, dashed lines are a guide for the eye. The vertical line at 373.2 K indicates the bulk BL038 T_c .

Figure 11. In-plane model of an H-PDLC layer showing the nanodroplets' size and shape distribution, their orientation within the layer and the temperature dependence of their internal director configuration.

At low temperature, the director configuration is dictated mainly by the confinement and independent from the magnetic field. At higher temperature, due to increased mobility, a fraction of the droplet, the larger in size, tend to align along the field, whereas another fraction, the smaller ones, becomes isotropic (see also text for details).

FIGURES

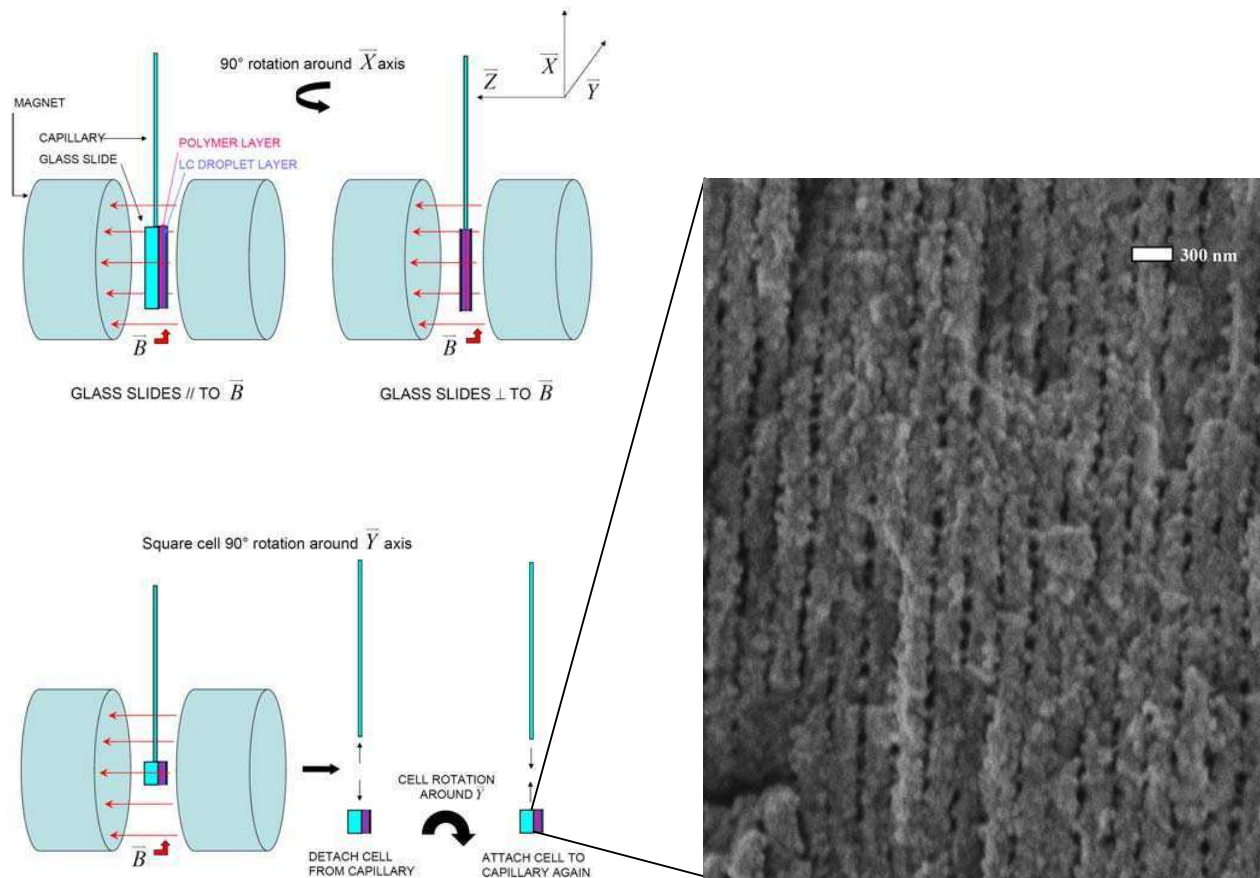


Figure 1:

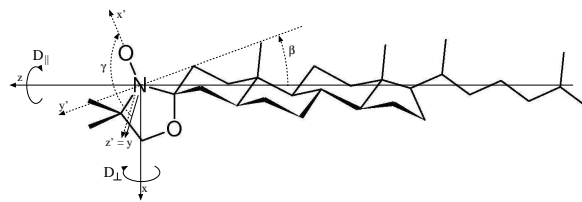


Figure 2:

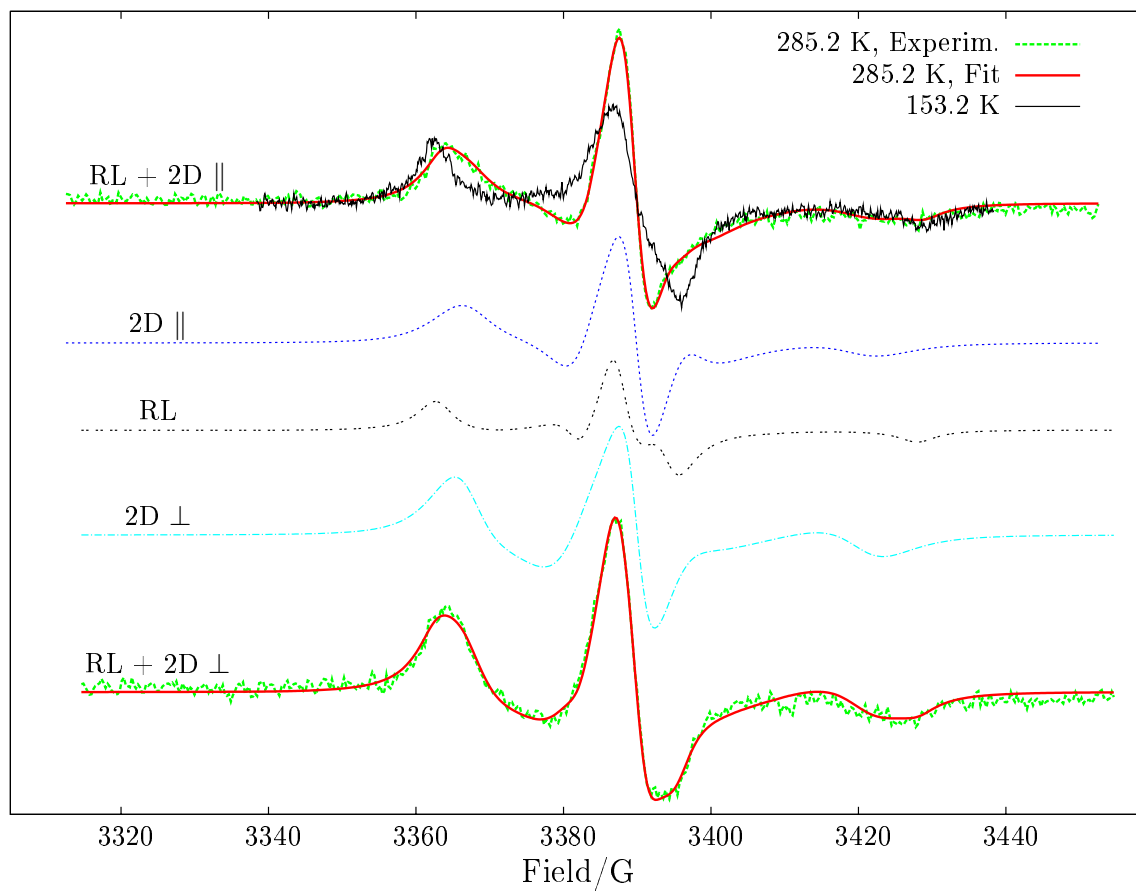


Figure 3:

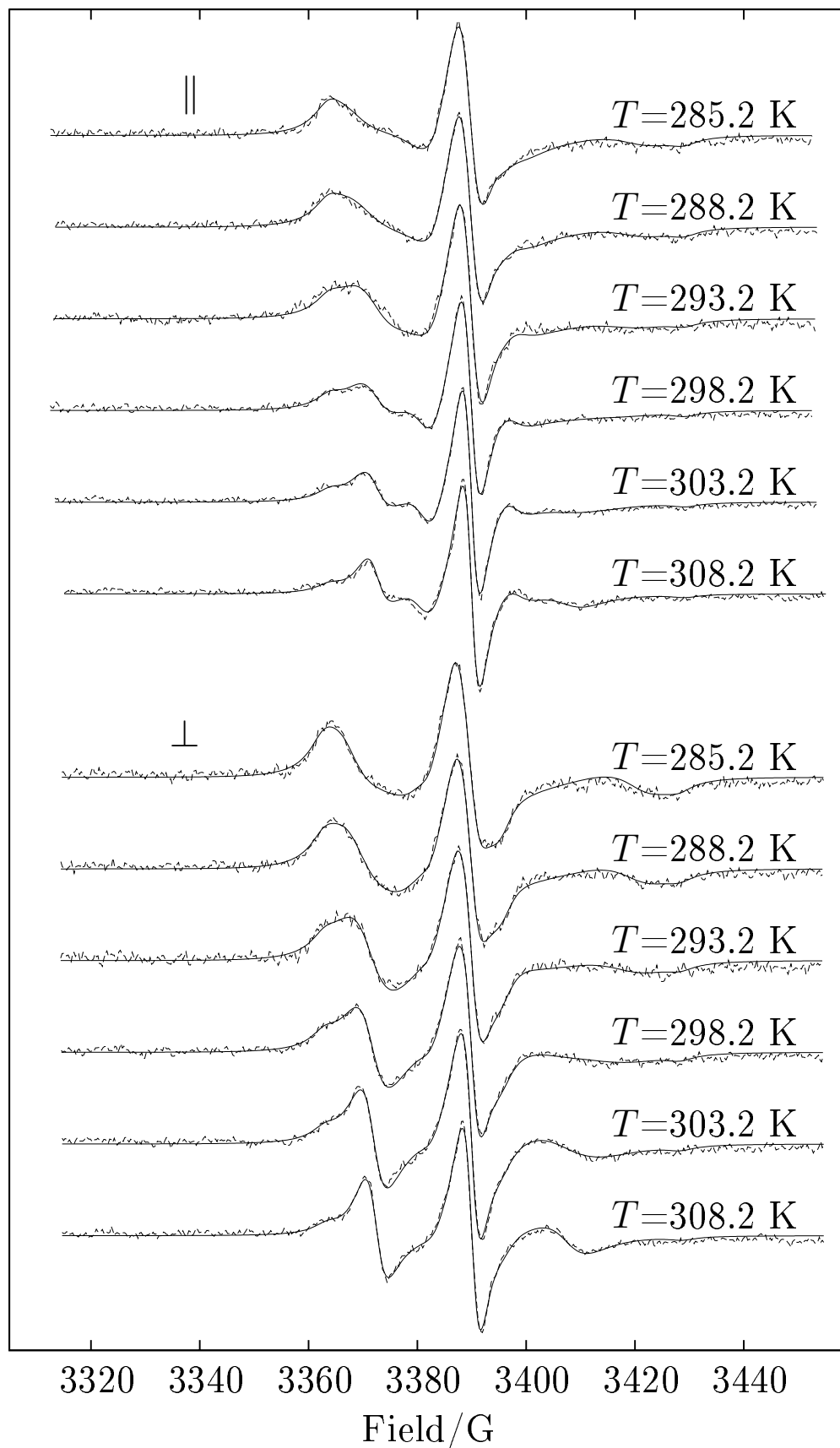


Figure 4:

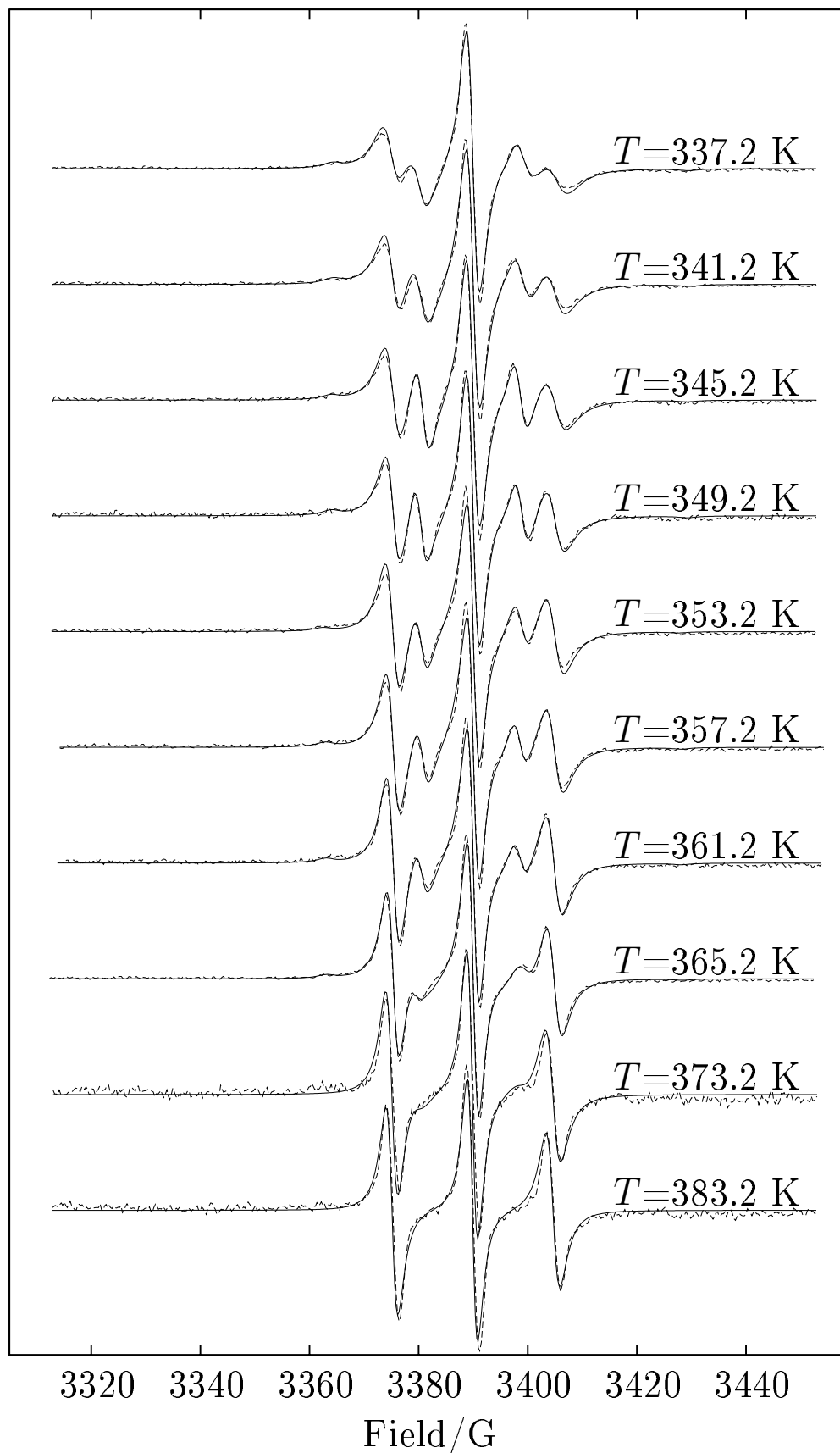


Figure 5:

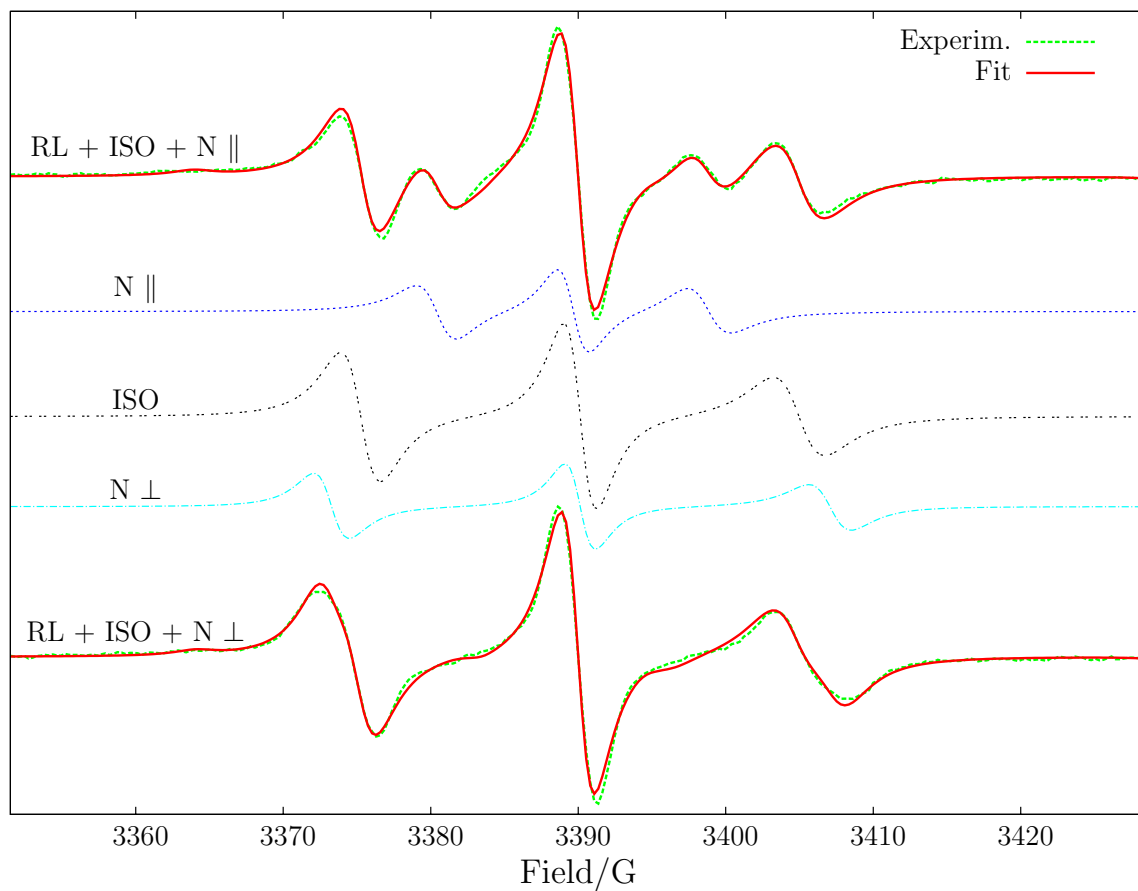


Figure 6:

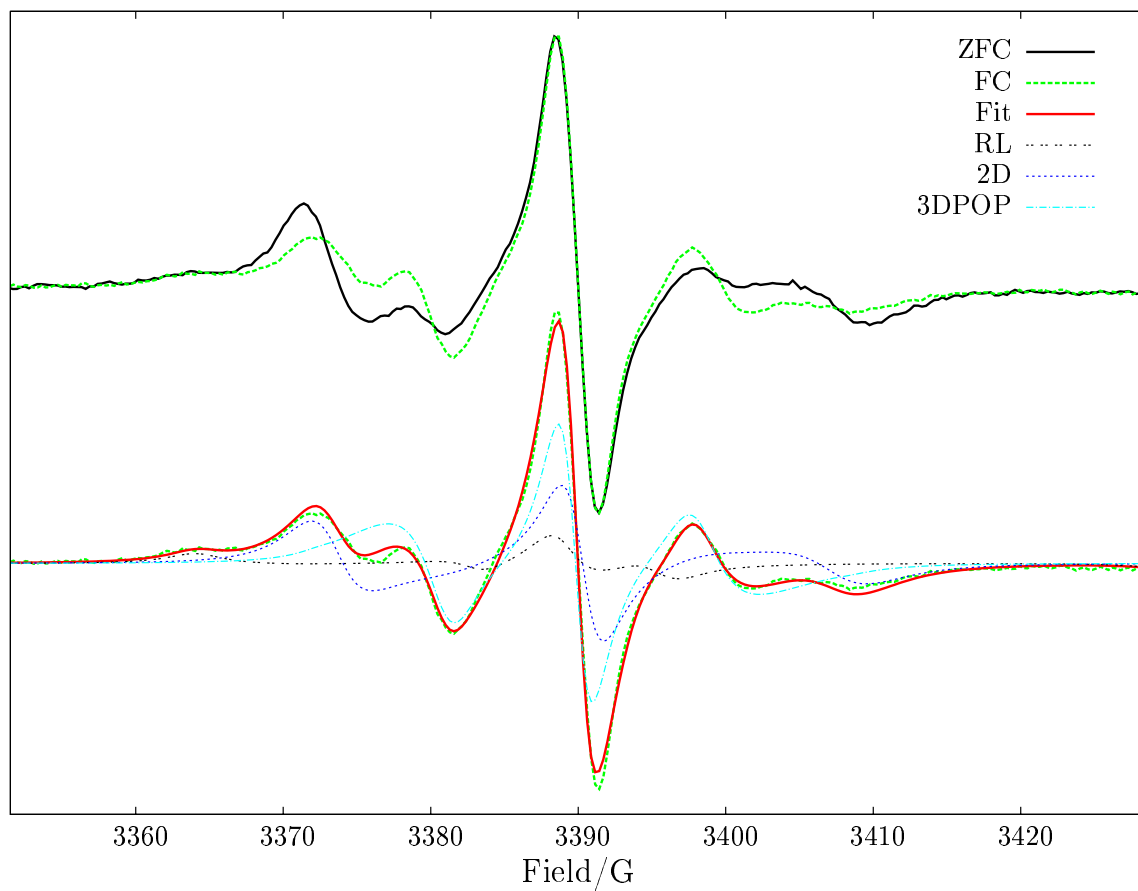


Figure 7:

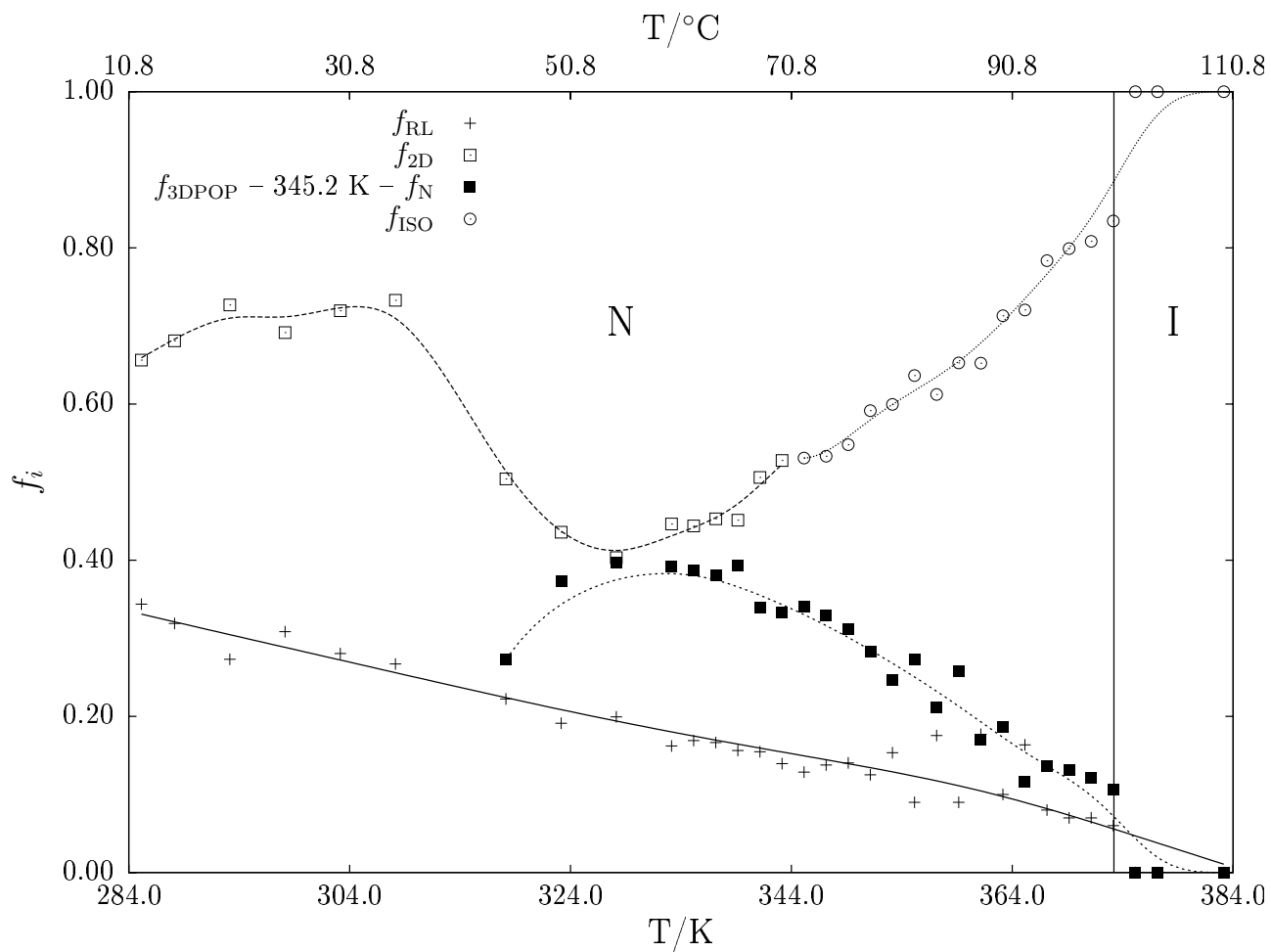


Figure 8:

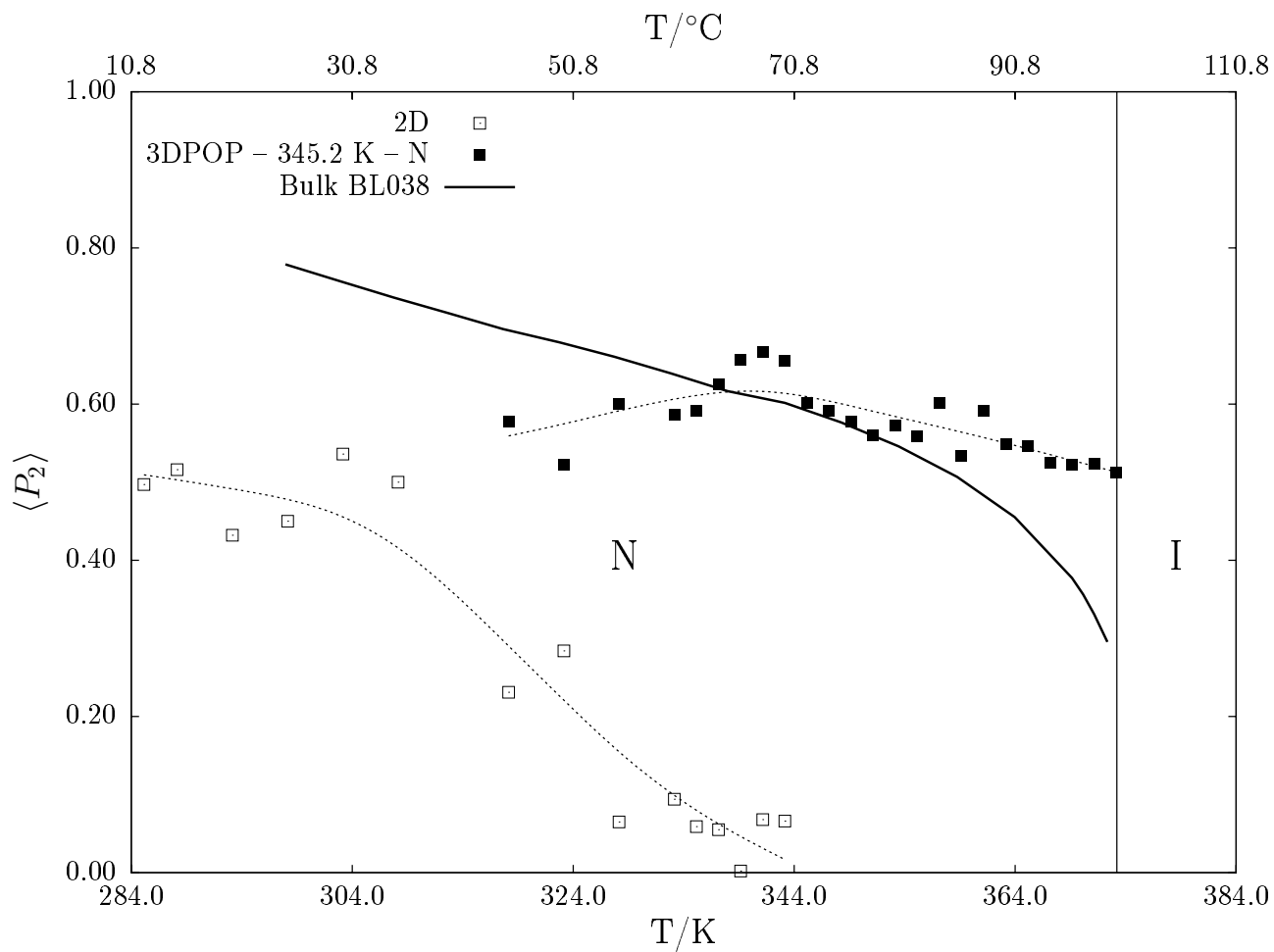


Figure 9:

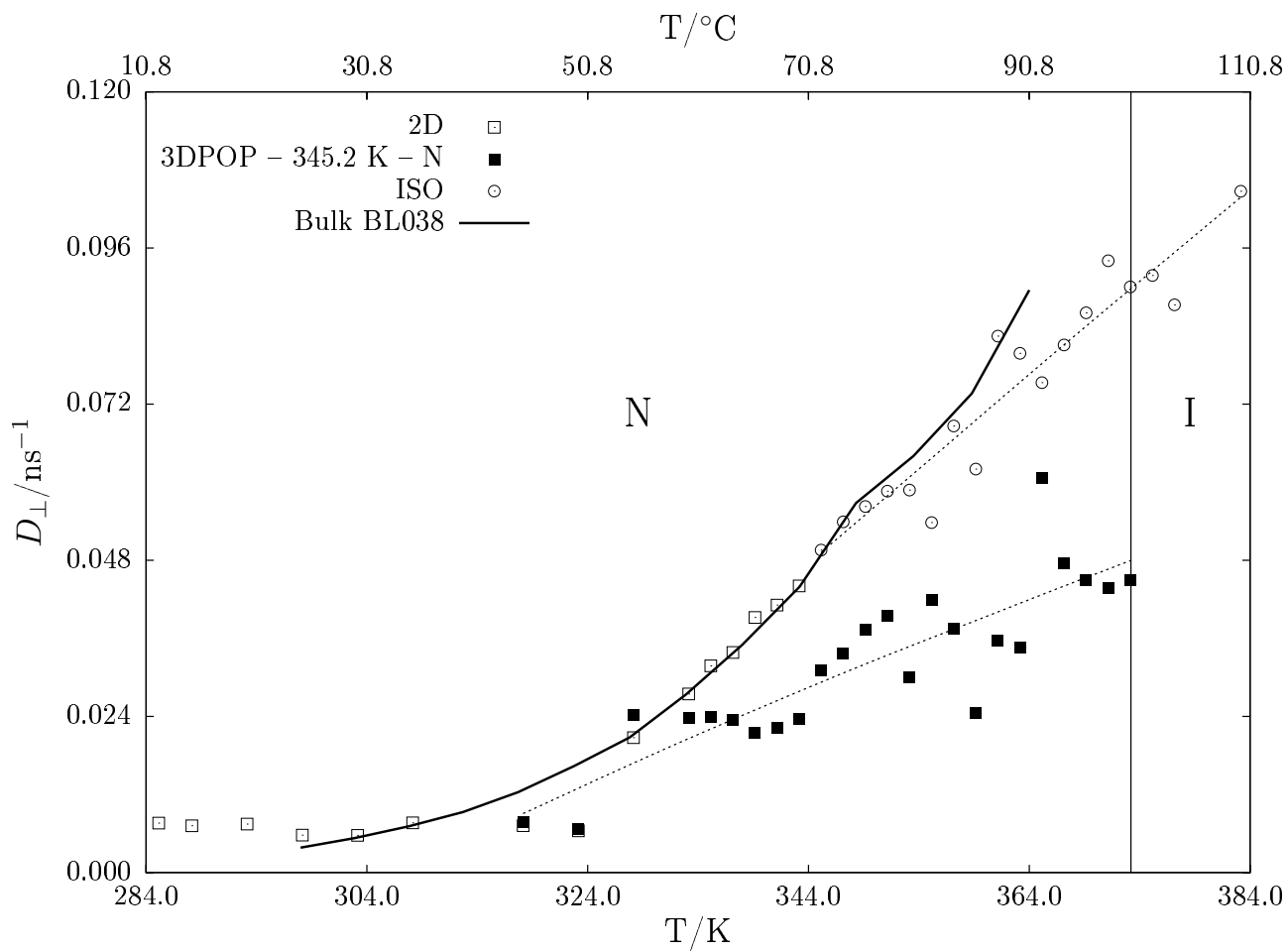
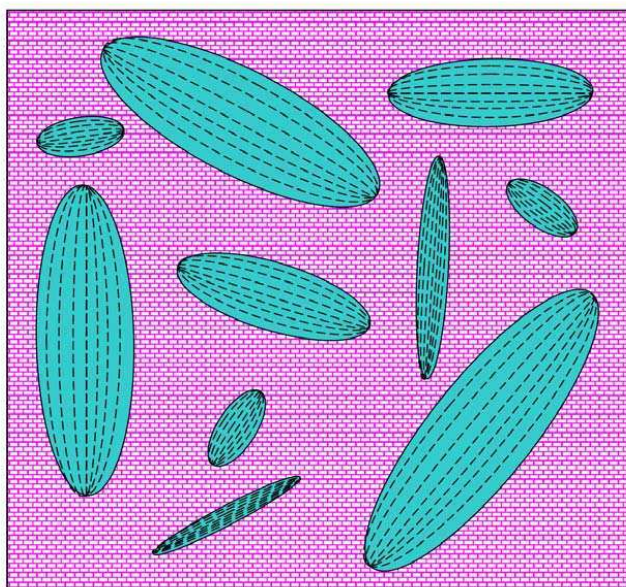


Figure 10:

Temperature range: 285 – 308 K



\bar{B}
←

Temperature range: 330 – 373 K

